Nonlinear Buckling Analysis of Composite Shells

P. SHARIFI*
Lockheed Missiles & Space Company, Inc., Sunnyvale, Calif.

An incremental finite element procedure is presented for nonlinear buckling (collapse) analysis of composite shells undergoing large elastic deformations. The type of element employed is a modified version of Clough-Felippa's quadrilateral shell element. The element is made of any number of rigidly bonded orthotropic layers of different thicknesses and material properties. Transverse shear deformations are neglected but the coupling between the inplane and bending, as well as between shear and normal deformations, is retained. A number of buckling problems of composite panels and shells are worked out and the results are presented.

I. Introduction

WITH the increasing applications of the multilayered composite materials in the aerospace industry, the need for computer-oriented solution techniques to handle composite constructions is quite apparent. To date, much effort has been directed toward development of computer programs based on the linear classical theory of orthotropic layered continuum. In this paper, a nonlinear finite element formulation is presented for the bending and buckling (collapse) analysis of laminated anisotropic shells undergoing large elastic deformations. The nonlinear collapse loads are obtained by the incremental applications of the loads up to the point where sudden jumps in the values of displacements are observed. Although the present derivation together with an eigensolution package is capable of predicting the bifurcation buckling loads, no detailed discussion of that is included here.

The type of element employed is a thin quadrilateral shell element. In the thickness direction, the element is assumed to be made of n number of rigidly bonded orthotropic layers of constant but different thicknesses. The composite thickness is assumed to be thin so that the Kirchhoff hypothesis is applicable. The layers can have different material properties and the principal axes of the material in each layer may have any orientation with respect to the element local coordinate axes. Hence, the composite lay-up is considered as an anisotropic laminate having coupling between the inplane and bending effects as well as between the shear and normal deformations.

This element is incorporated into a general three-dimensional, nonlinear finite element code called NEPSAP[1] which in addition contains beams, two- and three-dimensional membranes, and three-dimensional solids in its element library. Using this program, the nonlinear collapse behavior of a number of test cases and production-type problems with composite construction have been studied. The results and their comparisons with other available solutions are discussed at the end of the paper.

II. Element Characteristics

A typical quadrilateral composite shell element (Q-shell) is shown in Fig. 1. This is a modified version of the Clough-Felippa's linear quadrilateral shell element.[2] As shown, the element is composed of 4 linear curvature-compatible (LCCT-12) triangular elements (T-shells) having linearly varying inplane deformation properties. At the T-shell level, the three DOF associated with the mid-side node of the exterior edge, say 1–2, are kinematically condensed out through an averaging process. At the Q-shell level, 17 internal DOF associated with nodes 5–9 are statically condensed out resulting in a quadrilateral element with a total of 20 DOF in terms of element local (x, y, z) coordinates, or 24 DOF in terms of global (X, Y, Z) coordinates.[2]

A. Displacement Patterns

In terms of element local coordinates, the displacement functions of a T-shell may be symbolically represented as

$$u_1^0(x,y) = \underset{1\times 5}{\langle \phi_1 \rangle}\ \underset{5\times 1}{\{q_1\}} \tag{1a}$$

$$u_2^0(x,y) = \underset{1\times 5}{\langle \phi_2 \rangle}\ \underset{5\times 1}{\{q_2\}} \tag{1b}$$

$$u_3^0(x,y) = \underset{1\times 11}{\langle \phi_3 \rangle}\ \underset{11\times 1}{\{q_3\}} \tag{1c}$$

where u_1^0, u_2^0, and u_3^0 are, respectively, the inplane and transverse displacements of a generic point in the mid-surface of the T-shell; $\mathbf{q}_1$, $\mathbf{q}_2$ denote u_1^0, u_2^0 DOF at the 5 nodal points of T-shell, respectively; and $\mathbf{q}_3$ denotes u_3^0, θ_x, θ_y DOF at the 3 corner nodes plus θ_n (edge rotations) at the 2 mid-side nodes. In Eq. (1), ϕ_1 and ϕ_2 are quadratic functions, and ϕ_3 is a cubic function. In Ref. 2 these functions are given in terms of natural coordinates of the T-shell.

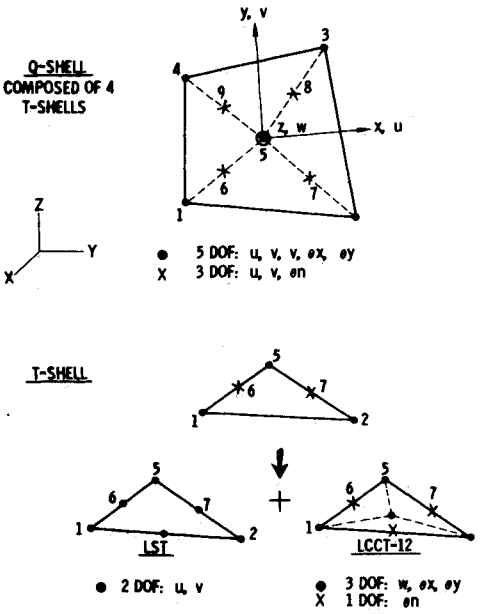

Fig. 1 A typical Q-shell element.

Presented as Paper 74-411 at the AIAA/ASME/SAE 15th Structures, Structural Dynamics and Materials Conference, Las Vegas, Nevada, April 17–19, 1974; submitted April 12, 1974; revision received December 4, 1974.

Index categories: Structural Composite Materials (including Coatings); Structural Stability Analysis; Structural Static Analysis.

* Research Specialist, Missile Systems Division. Member AIAA.

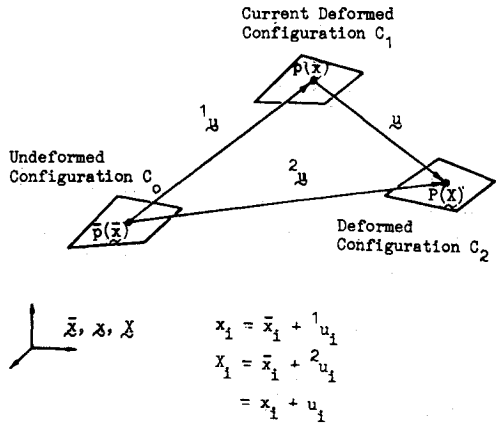

Fig. 2 Configurations of an element in its path of deformation.

Assuming Kirchhoff hypothesis, displacements at any point in the T-shell are defined as

$$u_\alpha(x,y,z) = u_\alpha{}^0 + zu_{3,\alpha}{}^0 \qquad (2a,b)$$

$$u_3(x,y,z) = u_3{}^0(x,y) \qquad (2c)$$

where z is the transverse local coordinate of T-shell with its origin at the mid-surface, $\alpha = 1,2$, and comma denotes differentiation, i.e., $(\ )_{,1} = \partial/\partial x$ and $(\ )_{,2} = \partial/\partial y$.

B. Strain-Displacement Relations

Three configurations of the Q-shell element in its path of deformation are shown in Fig. 2. Configuration C_0 denotes the undeformed state, and configurations C_1 and C_2 denote the deformed states of the element. State variables referred to C_1 and C_2 are denoted by left-superscripts 1 and 2, respectively, and the incremental quantities between C_1 and C_2 have no left-superscripts. Whenever indicial notation is used, summation convention applies and the Latin indices have a range of 1 to 3 and Greek indices 1 and 2.

In terms of a fixed rectangular coordinate system $\bar{x}_i$, $x_i = \bar{x}_i + {}^1u_i$ and $X_i = \bar{x}_i + {}^2u_i = x_i + u_i$ describe the positions of a generic material point in C_0, C_1 and C_2, respectively (see Fig. 2). Assuming $\bar{x}_i$ coincide with the element local coordinates in C_0 (i.e., $\bar{x}_1 = x$, $\bar{x}_2 = y$ and $\bar{x}_3 = z$) the displacement functions in Eqs. (2) applies to ${}^1u_i$, ${}^2u_i$ and $u_i = {}^2u_i - {}^1u_i$. Following the incremental Lagrangian finite element formulation,[1] where the undeformed configuration of the element is taken as the reference state, the incremental strain tensors in the element between configurations C_1 and C_2 are given by

$$\varepsilon_{\alpha\beta} = e_{\alpha\beta} + \eta_{\alpha\beta} \qquad (3)$$

where

$$2e_{\alpha\beta} = u_{\alpha,\beta} + u_{\beta,\alpha} + {}^1u_{m,\alpha}\,u_{m,\beta} + {}^1u_{m,\beta}\,u_{m,\alpha} \qquad (4a)$$

are the linear components and

$$2\eta_{\alpha\beta} = u_{m,\alpha}\,u_{m,\beta} \qquad (4b)$$

are the nonlinear components of Cartesian incremental strain tensor of the element. Here, u_m are the incremental components of the displacement vector and ${}^1u_m$ are the components of the total displacement vector of the element in C_1. Comma denotes differentiation with respect to the element local coordinates in C_0. Note that the existence of total deformation gradients, ${}^1u_m$, in Eq. (4a) is a consequence of adopting the element underformed configuration as the reference state. Substituting Eqs. (2) into Eqs. (4) and neglecting the nonlinear terms in z

$$e_{\alpha\beta} = e_{\alpha\beta}{}^0 + z\kappa_{\alpha\beta} \qquad (5a)$$

and

$$2\eta_{\alpha\beta} = u_{m,\alpha}{}^0 u_{m,\beta}{}^0 \qquad (5b)$$

where $e_{\alpha\beta}{}^0$ are the inplane strains, and $\kappa_{\alpha\beta}$ are the curvature tensors of a point in the middle surface of T-shell. Utilizing the element displacement functions (1) the following incremental strain-displacement relations are obtained.

$$\underset{3\times 1}{\begin{Bmatrix} e^0 \\ \cdots \\ \kappa \end{Bmatrix}} = \underset{3\times 10}{\begin{bmatrix} B_{\alpha\alpha} \\ \cdots \\ B_{3\alpha} \end{bmatrix}} \underset{3\times 11}{\begin{bmatrix} B_{\alpha 3} \\ \cdots \\ B_{33} \end{bmatrix}} \underset{11\times 1}{\begin{Bmatrix} q_\alpha \\ \cdots \\ q_3 \end{Bmatrix}} \qquad (6)$$

and

$$2\eta_{\alpha\beta} = \underset{1\times 21}{\{q\}^T}\ \underset{21\times 21}{[\Lambda_{\alpha\beta}]}\ \underset{21\times 1}{\{q\}} \qquad (7)$$

where

$$\{e^0\}^T = \langle e_{11}{}^0 e_{22}{}^0 2e_{12}{}^0 \rangle$$
$$\{\kappa\}^T = \langle \kappa_{11}\kappa_{22}2\kappa_{12} \rangle$$
$$\{q_\alpha\}^T = \langle q_1 \vdots q_2 \rangle$$
$$\{q\}^T = \langle q_1 \vdots q_2 \vdots q_3 \rangle$$
$$[\Lambda_{\alpha\beta}] = \langle \phi_{m,\alpha} \rangle^T \langle \phi_{m,\beta} \rangle,$$

and

$$\underset{3\times 10}{[B_{\alpha\alpha}]} = \begin{bmatrix} (1+g_{11})\langle \Phi_{1,1} \rangle + g_{21}\langle \Phi_{2,1} \rangle \\ (1+g_{22})\langle \Phi_{2,2} \rangle + g_{12}\langle \Phi_{1,2} \rangle \\ (1+g_{11})\langle \Phi_{1,2} \rangle + \\ \quad (1+g_{22})\langle \Phi_{2,1} \rangle + \\ \quad \langle g_{12}\Phi_{1,1} + g_{21}\Phi_{2,2} \rangle \end{bmatrix}$$

$$\underset{3\times 11}{[B_{\alpha 3}]} = \begin{bmatrix} g_{31}\langle \Phi_{3,1} \rangle \\ g_{32}\langle \Phi_{3,2} \rangle \\ g_{31}\langle \Phi_{3,2} \rangle + g_{32}\langle \Phi_{3,1} \rangle \end{bmatrix}$$

$$\underset{3\times 10}{[B_{3\alpha}]} = \begin{bmatrix} f_{11}\langle \Phi_{1,1} \rangle + f_{21}\langle \Phi_{2,1} \rangle \\ f_{22}\langle \Phi_{2,2} \rangle + f_{12}\langle \Phi_{1,2} \rangle \\ f_{11}\langle \Phi_{1,2} \rangle + f_{21}\langle \Phi_{2,2} \rangle + \\ \quad f_{22}\langle \Phi_{2,1} \rangle + f_{12}\langle \Phi_{1,1} \rangle \end{bmatrix}$$

$$\underset{3\times 11}{[B_{33}]} = \begin{bmatrix} (1+g_{11})\langle \Phi_{3,11} \rangle + g_{21}\langle \Phi_{3,21} \rangle \\ (1+g_{22})\langle \Phi_{3,12} \rangle + g_{12}\langle \Phi_{3,12} \rangle \\ (1+g_{11})\langle \Phi_{3,12} \rangle + \\ \quad (1+g_{22})\langle \Phi_{3,21} \rangle + \\ \quad \langle g_{21}\Phi_{3,22} + g_{12}\Phi_{3,11} \rangle \end{bmatrix}$$

where

$$g_{m\alpha} = {}^1u_{m,\alpha}{}^0, \qquad f_{\alpha\beta} = {}^1u_{3,\alpha\beta}$$

The existence of total deformation gradients ($g_{m\alpha}$ and $f_{\alpha\beta}$) in the B matrix, which results in the coupling between the curvature and inplane deformations, is a consequence of adopting the undeformed configuration of the element as the reference state (Lagrangian formulation).

C. Lay-Up Constitutive Relations

In each layer, in terms of element local coordinate system, the incremental stress-strain relations including thermal effects can be written as

$$\underset{3\times 1}{\{s\}_k} = \underset{3\times 3}{[C]_k}\ \underset{3\times 1}{\{e\}_k} - \theta_k\ \underset{3\times 1}{\{\lambda\}_k} \qquad (8)$$
$$k = 1,2,\ldots,n$$

where $\{s\}^T = \langle s_{11}s_{22}s_{12} \rangle$ are the incremental Piola stress tensors expressed in terms of area and coordinates of element in C_0, $[C]$ is in general a full 3×3 two-dimensional (plane stress) modulus matrix in terms of element local coordinates, and

$$\{e\}_k = \{e^0\} + z_k\{\kappa\} \qquad (9a)$$

$$\theta_k = \theta_0 + z_k G \qquad (9b)$$

$$\{\lambda\}_k = [C]_k\{\alpha\}_k \qquad (9c)$$

where θ_0 and G are the increments of inplane temperature and temperature gradients at the mid-surface, respectively; $\{\alpha\}^T = \langle \alpha_{11}\alpha_{22}\alpha_{12} \rangle$ are the coefficients of thermal expansion in terms of element local coordinates. When the material principal axes coincide with the element local axes $\alpha_{12} = 0$ and $C_{13} = C_{23} = C_{31} = C_{32} = 0$; $z_k = \frac{1}{2}(h_k + h_{k-1})$ and h_k are shown in

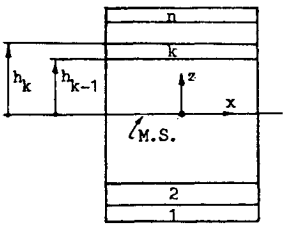

Fig. 3 Lay-up configuration.

Fig. 3. In Eqs. (8) and (9) the subscript k denotes a typical layer number and it ranges from 1–n (maximum number of layers). Figure 3 also shows the stacking order of the lay-up.

To get the element effective constitutive relation, Eqs. (8) are integrated over the composite thickness resulting in

$$\underset{\substack{3\times1\\3\times1}}{\begin{Bmatrix}N\\M\end{Bmatrix}} = \underset{\substack{3\times3 & 3\times3\\3\times3 & 3\times3}}{\begin{bmatrix}D_{11} & D_{12}\\D_{21} & D_{22}\end{bmatrix}} \underset{\substack{3\times1\\3\times1}}{\begin{Bmatrix}e^0\\\kappa\end{Bmatrix}} - \underset{\substack{3\times1\\3\times1}}{\begin{Bmatrix}N_T\\M_T\end{Bmatrix}} \tag{10}$$

where $\{N\}^T = \langle N_{11}N_{22}N_{12}\rangle$ and $\{M\}^T = \langle M_{11}M_{22}M_{12}\rangle$ are the resultant force and moment, respectively,

$$\begin{Bmatrix}N_T\\M_T\end{Bmatrix} = \begin{bmatrix}D_{11} & D_{12}\\D_{21} & D_{22}\end{bmatrix} \begin{Bmatrix}\theta_0 & \{\alpha\}\\G & \{\alpha\}\end{Bmatrix} \tag{11a}$$

are the resultant thermal effects, and

$$D_{11} = \sum_{k=1}^{n} [C]_k(h_k - h_{k-1}) \tag{11b}$$

$$D_{12} = D_{21}{}^T = \frac{1}{2}\sum_{k=1}^{n} [C]_k(h_k{}^2 - h_{k-1}{}^2) \tag{11c}$$

$$D_{22} = \frac{1}{3}\sum_{k=1}^{n} [C]_k(h_k{}^3 - h_{k-1}{}^3) \tag{11d}$$

D. Equilibrium Equations

The nonlinear solution is obtained through a step-by-step incremental method. At the start of each solution step, a new set of equilibrium equations are computed for each element relating the incremental displacements to the incremental loads. Equations (10) and (11) are derived using an incremental virtual work expression[1] where the undeformed configuration of the element (configuration C_0 in Fig. 2) is taken as the reference configuration (Lagrangian formulation).

Utilizing the element displacements functions (1) together with the kinematical and constitutive relations (6, 7, 10, and 11) the previous variational expression as applied to the present element between configurations C_1 and C_2 can be written as

$$\delta\{q\}^T\{Q\} = \delta\{q\}^T[K_0 + K_g]\{q\} \tag{12}$$

where

$$\{Q\} = \int_{a_0} [\phi]^T\{p\}da_0 + \int_{a_0} [B]^T \begin{Bmatrix}N_T\\M_T\end{Bmatrix} da_0 \tag{13a}$$

$$[K_0] = \int_{a_0} [B]^T[D][B]da_0 \tag{13b}$$

$$[K_g] = \frac{1}{2}\int_{a_0} {}^1N_{\alpha\beta}[\Lambda_{\alpha\beta} + \Lambda_{\beta\alpha}]da_0 \tag{13c}$$

Since $\delta\{q\}$ are arbitrary variational quantities, they can be deleted from both sides of Eq. (12) to give

$$\underset{21\times1}{\{Q\}} = \underset{21\times21}{[K_0 + K_g]}\ \underset{21\times1}{\{q\}} \tag{14}$$

which is the T-shell incremental equilibrium equation in terms of element local coordinates. Here $\{Q\}$ is the load vector, K_0 and K_g are, respectively, the ordinary and geometric stiffness matrices. In Eqs. (13), $\{p\}^T = \langle p_1p_2p_3\rangle$ is the incremental surface traction vector, $[\phi]$ is the matrix of displacement functions ϕ_1, ϕ_2 and ϕ_3, Eq. (1); a_0 is the area of T-shell in C_0 and the integrals are evaluated numerically.

Equations (14) are formed for the 4 T-shells individually. After transforming these equations to the global coordinates, they are assembled to form the equilibrium equations of the Q-shell. Then the internal DOF associated with the interior nodes 5–9 are statically condensed out resulting in a quadrilateral element with 24 DOF in terms of global coordinates.

For equilibrium correction through one or more cycles of iteration after each incremental step, the effective T-shell load vector may be computed using

$$\underset{21\times1}{\{Q_e\}} = \int_{a_0} [B]^T \begin{Bmatrix}{}^1N\\{}^1M\end{Bmatrix} da_0 \tag{15}$$

where B is the strain-displacement matrix defined in Eq. (6) and $\{{}^1N\}^T = \langle {}^1N_{11}{}^1N_{22}{}^1N_{12}\rangle$ and $\{{}^1M\}^T = \langle {}^1M_{11}{}^1M_{22}{}^1M_{12}\rangle$ are, respectively, the resultant force and moment in the element in current configuration, C_1. After the appropriate transformation and assembly, these loads are subtracted from the total applied loads to get the out-of-balance forces which are needed for iteration purposes.

For bifurcation buckling load predictions at any load step, the ordinary and geometric stiffness matrices may be assembled separately and the resulting eigenproblem; i.e., $(K_0 - \omega K_g)$, solved for the lowest eigenvalue (critical load) and its associated eigenvector (buckling mode).

III. Nonlinear Collapse Analysis

The foregoing formulation is capable of analyzing the nonlinear bending and buckling behavior of general shells of composite construction. For the prediction of nonlinear buckling (collapse) loads, the loads are applied incrementally up to the point where either: a) negative term(s) on the diagonal of the structural stiffness matrix is (are) formed, or b) sudden jumps in the values of the deflections are obtained. The latter situation indicates the total collapse of the structure, while condition a), in the absence of large deflections, may indicate any of the following possibilities: local buckling in the case of complex geometries, or ill conditioning of the equations due to an irregular mesh lay-out and/or large load-step sizes. The ill-conditioning possibility is specially true with low accuracy computer systems. One relatively inexpensive way of remedying this situation is to re-run the last one or two increments taking smaller load-steps.

IV. Numerical Examples

The subject composite element has been incorporated into NEPSAP which is a three-dimensional nonlinear finite element code. This program is capable of handling structures composed of beams, membranes, three-dimensional solids, monocoque and composite shells or any combination of them undergoing large elastic-plastic deformations.[1] Using NEPSAP, a number of nonlinear collapse problems of composite shells and panels have been analyzed. In the following, the results of 3 of these problems together with experimental and analytical data available are presented.

A. Composite Panels under Axial Compression

The buckling strengths of 5 10×10-in. composite panels under axial compression were investigated. The panels are clamped (C) at the loaded edges and clamped or simply supported (SS) at the other two edges. The composite lay-up consists of 20 layers of 0.0051 in. thick boron-epoxy with the following orthotropic material data: $E_{11} = 30{,}900$ ksi, $E_{22} = 2{,}500$ ksi, $G_{12} = 1000$ ksi, and $\nu_{12} = 0.28$. In each panel, the material axes of the layers are oriented at different angles with respect to the axis of the load,[3] but symmetrical about the midsurface. To determine the nonlinear collapse load, which should also coincide with the bifurcation buckling load, a small lateral load of the order of ($10^{-4}\times$ buckling load) was applied at the center of each panel to trigger out-of-plane displacements. The resulting finite element solution together with the experimental and analytical (bifurcation load) predictions reported in Ref. 3

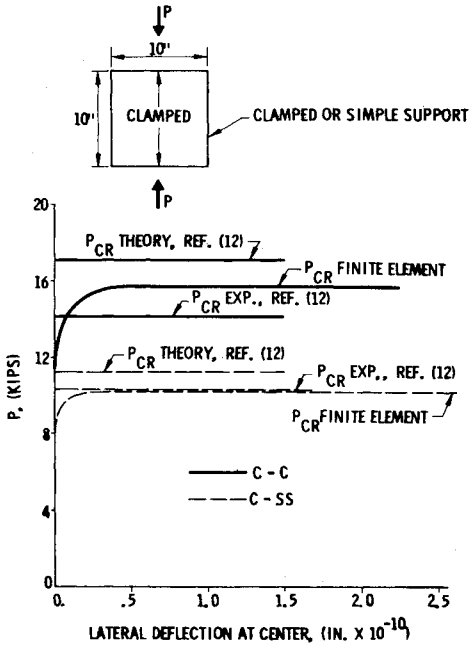

Fig. 4 Load vs deflection of a composite panel.

for the panel No. 1 are shown in Fig. 4. Similar results for the other 4 panels were obtained. These results are summarized in Fig. 5. As shown a very satisfactory correlation between the finite element results and those published by Ref. 3 is achieved. In this study, the panels were modeled by a 3×4 finite element mesh.

B. Post-Buckling of a Shear Panel

The post-buckling diagonal tension behavior of a 6×18-in. composite shear panel clamped on each edge by a pin connected frame as shown in Fig. 6 was investigated. The panel is made of 4 layers of $\pm 45°$ symmetrically stacked boron-epoxy material with $E_{11} = 31{,}000\,\text{ksi}, E_{22} = 3{,}000\,\text{ksi}, G_{12} = 1{,}100\,\text{ksi}, \nu_{12} = 0.22$ and a thickness of 0.005 in. This is one of the test specimens used in the experimental investigation reported in Ref. 4. The finite element mesh, loading and boundary conditions used in the present nonlinear analysis are shown in Fig. 6. As shown, the panel is subjected to an inplane diagonal force P. To trigger the out-of-plane buckling modes, a small lateral force of $Q = P/10{,}000$ was applied at the center of panel, Fig. 6. The finite element solution together with the experimental and analytical (linear buckling load) results of Ref. 4 are plotted in Fig. 7. A surprisingly good correlation is achieved between the finite element and experimental maximum-deflections. As shown, near the value of linear buckling load[4] ($P = 303$ lb)

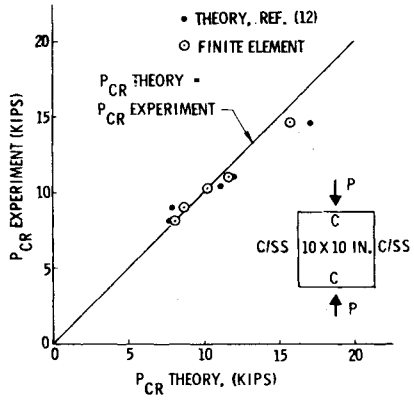

Fig. 5 Buckling loads of composite panels.

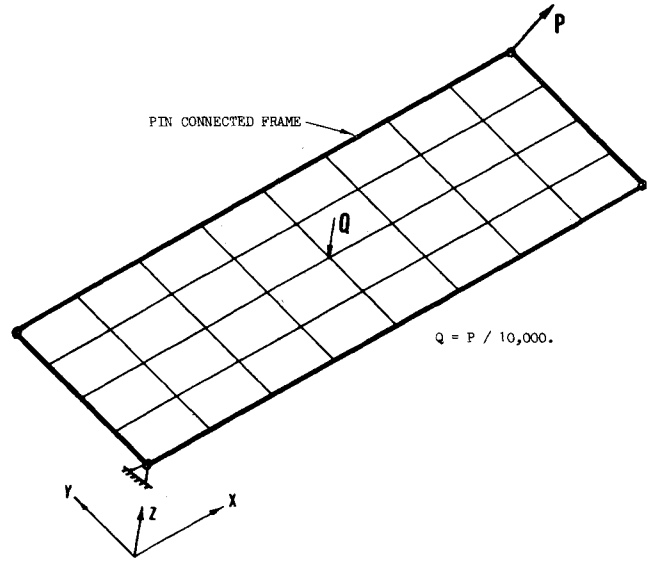

Fig. 6 $(45,-46)_s$ composite boron-epoxy shear panel 6×18.

the transverse deflections increase rapidly. This coincides with the formation of diagonal wave patterns (not shown) which causes the panel to carry the load as a diagonal tension member (truss) in the post-buckling region. The finite element solution also indicates that the panel does not collapse, but rather it stiffens up as the load is increased further above the bifurcation point. This result is also indicated by the experimental data which shows the panel fails at five times the bifurcation load due to tearing at the corners.[4]

C. Ring-Stiffened Composite Cone

The cone shown by dotted lines in Fig. 8 is a ring-stiffened sandwich structure supported by a monocoque cylindrical skirt. The sandwich construction is made of aluminum honeycomb core with composite face sheets. The nonlinear collapse load of this structure was investigated using 2 finite element models a) and b) shown in Figs. 8a and 8b, respectively. Model a) is a coarse mesh with the sandwich core and facings modeled by multilayered composite elements. This model neglects the effect of transverse shear deformations of the honeycomb core on the collapse load. To study the extent of this effect, model b) was constructed. In this model the sandwich construction was modeled "exactly" using three-dimensional orthotropic solid elements for the core and composite

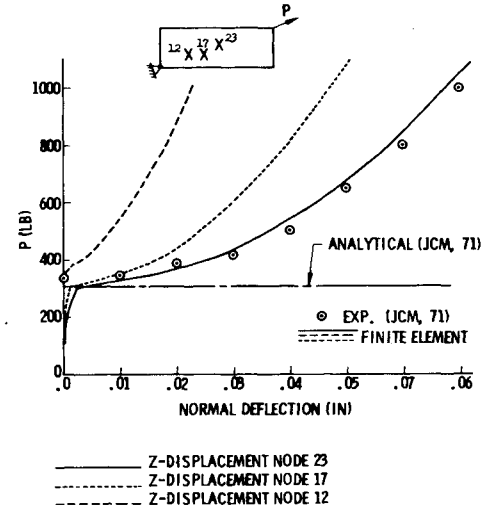

Fig. 7 Post-buckling of a composite shear panel.

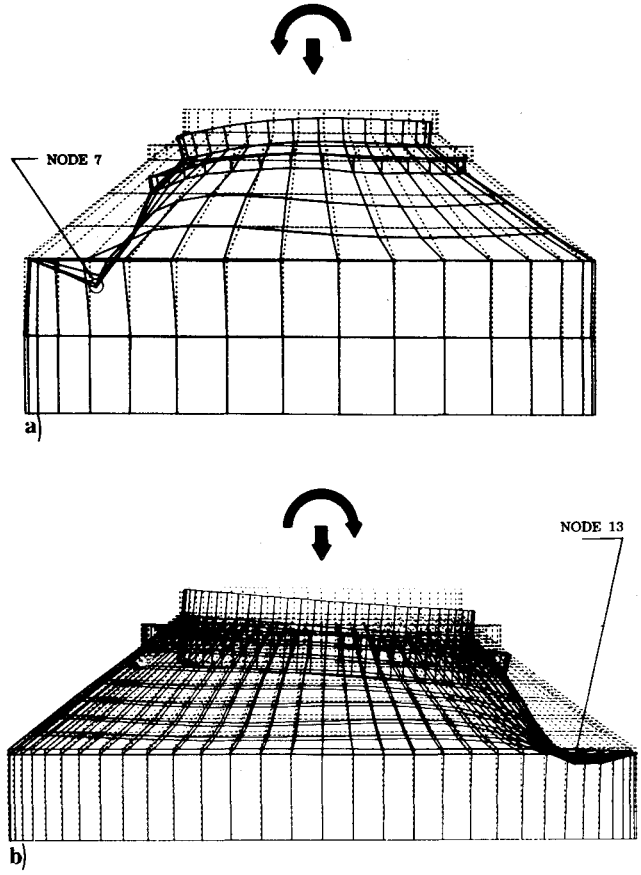

Fig. 8 Buckling mode of cones.

Q-shell elements for the facings. The cone is subjected to axial and flexural loadings which were applied as equivalent point loads around the top circumference. Because of planar symmetry, only half the structure (180°), shown in Fig. 8, was considered for both models.

The results of this study are shown in Figs. 8 and 9. Figures 8a and 8b show the collapse modes, and Fig. 9 shows the load-deflection characteristics of the two models. As shown in Fig. 9, the collapse occurs at a load factor of 4.0 for model a) and 2.8 for model b). This indicates a 30% drop in the value of collapse load as a result of shear deformation in the core. For model a), the bifurcation buckling load of the smeared

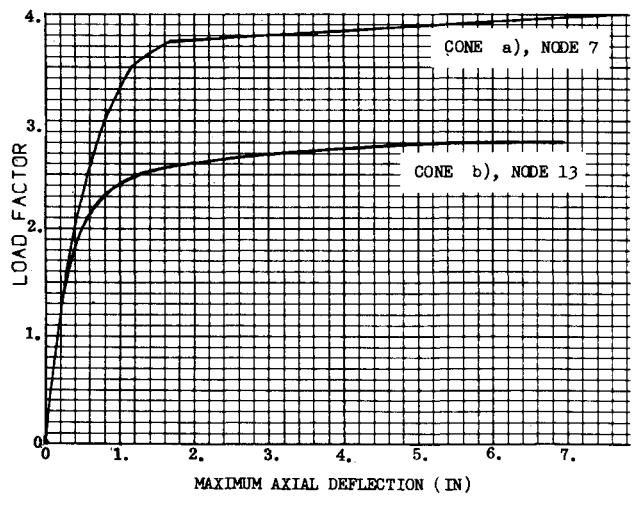

Fig. 9 Load deflections of cones a and b.

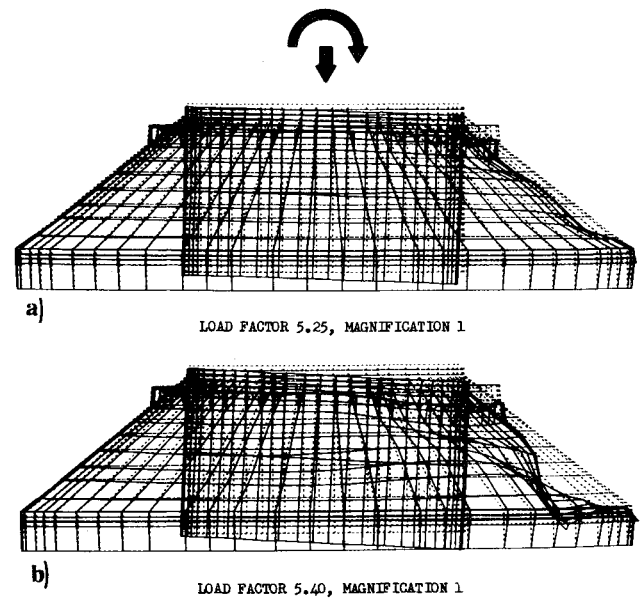

Fig. 10 Deflected shape of cone c at a load factor of a) 5.25 and b) 5.4.

cone was studied using the BOSOR[5] finite difference code. An eigenvalue analysis was carried out. The bifurcation point was predicted to lie at a load factor of 4.5 which is 12.5% higher than the collapse load calculated by the finite element analysis.

More recently, a slightly different configuration of the cone with cutouts was analyzed using the finite element model shown in Fig. 10. The collapse mode of this cone, designated as cone c), is shown in Fig. 10b. Figure 10a shows its deflected shape obtained at 3% below the collapse load. A comparison of the deflected shapes shown in Fig. 10 indicates the highly nonlinear nature of this problem. Collapse loads for models a), b), and c) were obtained using 9, 14 and 15 increments, respectively, as shown in Table 1.

V. Conclusions

The last two examples discussed in this paper clearly indicate the importance of nonlinear large displacement analytical approach for the buckling (collapse) analysis of structural systems. In example 2, the linear buckling results were totally misleading, and in example 3, the linear bifurcation prediction was nonconservative. Although the nonlinear solutions are generally more time-consuming and costly as compared to the conventional linear solutions, the degree of accuracy and reliability achieved by a nonlinear approach warrants its use for the stress and buckling analysis of a wide range of structural problems. One such method as applied to the composite shell-type structures using finite element technique was discussed. This capability

Table 1 Summary of size and run times for models a, b and c

	Model a	Model b	Model c
Nodes	180	792	932
Equations	920	3,976	4,753
Band width (ave.)	60	167	174
Elements:			
Beams	102	256	155
Monocoque Q-shell	69	128	120
Composite Q-shell	119	673	776
Three-dimensional solids	...	256	268
UNIVAC-1108 run time per increment CPU (min.)	3.4	23	29

has been incorporated into a production oriented three-dimensional finite element code called NEPSAP. Applications of the code for the collapse analysis of a number of classical and production-type problems with composite construction were illustrated.

References

[1] Sharifi, P. and Yates, D. N., "Nonlinear Thermo-Elastic-Plastic and Creep Analysis by the Finite Element Method," *AIAA Journal*, Vol. 12, Sept. 1974, pp. 1210–1215.

[2] Clough, R. W. and Felippa, C. A., "A Refined Quadrilateral Element for Analysis of Plate Bending," *Proceedings of Second Conference on Matrix Methods in Structural Mechanics*, AFFDL-TR-68-150, Oct. 1968, Air Force Flight Dynamics Lab., Wright-Patterson Air Force Base, Ohio, pp. 399–440.

[3] Suarez, J. A., "Advanced Composite Wing Structures, Stability Analysis of Advanced Filamentary Composite Panels," Tech. Rept. AC-SM-8087, May 1970, Grumman Aircraft Engineering Corp., Bethpage, N.Y.

[4] Kaminski, B. E. and Ashton, J. E., "Diagonal Tension Behavior of Boron-Epoxy Shear Panels," *Journal of Composite Materials*, Vol. 5, Oct. 1971, pp. 553–558.

[5] Bushnell, D., "Stress, Stability, and Vibration of Complex Branched Shells of Revolution: Analysis and User's Manual for BOSOR4," LMSC-D243605, March 1972, Lockheed Missiles & Space Co., Sunnyvale, Calif. Also CR 2116, Oct. 1972, NASA.

JUNE 1975 AIAA JOURNAL VOL. 13, NO. 6

Fracture Mechanics Application of an Assumed Displacement Hybrid Finite Element Procedure

SATYA N. ATLURI*
Georgia Institute of Technology, Atlanta, Ga.
AND
ALBERT S. KOBAYASHI† AND MICHIHIKO NAKAGAKI‡
University of Washington, Seattle, Wash.

An assumed displacement hybrid finite element procedure developed specifically for treating mixed-mode behavior of cracks was used to solve two-dimensional problems in fracture mechanics involving anisotropic, nonhomogeneous but linearly elastic materials. The procedure was then checked by analyzing problems with known solutions which include centrally cracked isotropic and orthotropic tension plates, single-edge-notched tension plate, oblique edge-notched tension plate, and tension plates with one-quarter circular crack and subjected to uniaxial or biaxial tension. Also a doubly edge-cracked orthotropic tension plate and an orthotropic three point bend specimen, for which theoretical solutions are not available, were analyzed.

I. Introduction

DURING the past decade fracture mechanics has been successfully used to analyze failed parts,[1,2] certifying a structure for its intended use,[3] and correlating cyclic or sustained stress crack growth[4] of flaws. In applying fracture mechanics to practical problems, however, the analyst must know the stress intensity factor of a flawed structure as well as the stress intensity factors of laboratory specimens used to establish material characteristics such as the fracture toughness, cyclic crack growth rates, and sustained stress crack growth rates. Unfortunately, available solutions of stress intensity factors are limited to idealized flaws of simple geometries and loading conditions and thus require considerable engineering judgment before they can be used to estimate stress intensity factors of complex flaws which exist in actual problems. It is also short of impossible to solve these practical problems by the elegant but laborious analytical procedures used by others.[5]

For two-dimensional problems in fracture mechanics, the method of finite element analysis which is a well-developed and widely used numerical technique in structural analysis[6] can be used to determine the stress intensity factor for a single mode,[7–12] as well as mixed mode of crack-tip deformation. For such elastic analysis, the stress singularity at the crack tip requires that small elements be used in the vicinity of the crack tip if the near-field stresses are to be accurately calculated. To circumvent such refinement, crack opening displacements[7,8] and more recently the strain energy release rate[9,10] have been used to estimate stress intensity factors with relatively coarse finite element grids. Although the crack opening displacement (COD) approach enables one to determine the opening mode and sliding mode stress intensity factors, the numerical accuracy of this approach leaves much to be desired. On the other hand, the approach by elastic strain energy release rate provides better accuracy but the two modes of crack-tip deformation cannot be separated.

Other approaches in determining the stress intensity factors by the method of finite element analysis involve developing super elements with various embedded stress singularity.

Presented as Paper 74-390 at the AIAA/ASME/SAE 15th Structures, Structural Dynamics and Materials Conference, Las Vegas, Nevada, April 17–19, 1974; submitted April 12, 1974; revision received November 22, 1974. The authors wish to express their gratitude to W. J. Walker, Air Force Office of Scientific Research, for his continuous support and encouragement. This work was supported by the Air Force Office of Scientific Research under Grant AFOSR-73-2478.

Index category: Structural Static Analysis.

* Associate Professor, School of Engineering Science and Mechanics.

† Professor, Department of Mechanical Engineering.

‡ Graduate Student, Department of Mechanical Engineering. Presently, Post Doctoral Fellow at Georgia Institute of Technology.